This is a preprint, the final version is subject to change, of the American Mineralogist (MSA)
Cite as Authors (Year) Title. American Mineralogist, in press.
(DOI will not work until issue is live.) DOI: http://dx.doi.org/10.2138/am-2017-5870

Revision 3

Experimental constraints on the stability of baddeleyite and zircon in carbonate- and silicate-carbonate melts

Fernanda Gervasoni*[1]; Stephan Klemme[1]; Arno Rohrbach[1]; Tobias Grützner[1]; Jasper Berndt[1]

[1] Institut für Mineralogie, Westfälische Wilhelms Universität, Corrensstrasse 24, 48149 Münster

*Corresponding author: gervasoni.fe@uni-muenster.de

Abstract

Carbonatites are rare igneous carbonate-rich rocks. Most carbonatites contain a large number of accessory oxide, sulfide and silicate minerals. Baddeleyite (ZrO_2) and zircon ($ZrSiO_4$) are common accessory minerals in carbonatites and as these minerals host high concentrations of U and Th, they are often used to determine the ages of formation of the carbonatite. In an experimental study we constrain the stability fields of baddeleyite and zircon in Ca-rich carbonate melts with different silica concentrations. Our results show that SiO_2-free and low silica carbonate melts crystallize baddeleyite, whereas zircon only crystallizes in melts with higher concentration of SiO_2. We also find that the zirconsilicate baghdadite ($Ca_3ZrSi_2O_9$) crystallizes in intermediate compositions. Our experiments indicate that zircon may not be a primary mineral in a low-silica carbonatite melt and care must be taken when interpreting zircon ages from low-silica carbonatite rocks.

Keywords: carbonatite, baddeleyite, baghdadite, zircon, silicate-carbonate melt, experimental petrology

Introduction

Carbonatites are rare igneous carbonate-rich rocks. Their genesis is still under debate and the most popular models involve partial melting from a CO_2-rich peridotite (Wallace and Green 1988; Sweeney 1994; Harmer and Gittins 1998), differentiation of CO_2-rich silicate melts (Gittins 1988; Gittins and Jago 1998), liquid immiscibility (Kjarsgaard and Hamilton 1988; Brooker and Kjarsgaard 2011), or a combination of the aforementioned processes.

Carbonatites occur usually in continental cratons related to rifting zones (Gittins 1988), and are often associated with silica undersaturated and alkaline rocks, e.g. phonolites, ijolites, or syenites. Although widespread in these tectonic settings, carbonatites are volumetrically small but they can contain economically important ore minerals (Mariano 1989). Carbonatites are known for their low viscosity (Dobson et al. 1996; Kono et al. 2014) and excellent wetting properties (Minarik and Watson 1995), which makes them effective metasomatic agents in the Earth's mantle (Wallace and Green 1988; Yaxley et al. 1991; Klemme et al. 1995).

Le Maitre defined carbonatite as rocks that contain 50% carbonate minerals and less than 20 wt.% of SiO_2 (Le Maitre 2002) and this is the basis for the IUGS classification of carbonatites. However, it was noted subsequently that with this classification many 'carbonatite-like' rocks are out of the carbonatite range, leading Mitchell (2005) to divide carbonatites into two groups: (1) calcite and/or dolomite carbonatites that are primary and genetically related to magmas originated in the mantle and (2) 'carbothermal' residua derived from a wide variety of magmas.

Carbonatites are known to host a large number of unusual oxide and silicate accessory minerals, including pyrochlore, perovskite, titanite, baddeleyite or zircon. As both zircon and baddeleyite can incorporate large amounts of U and Th, these minerals are commonly employed to determine the ages of formation of the carbonatites (e.g., Heaman and LeCheminant 1993; Reischmann et al. 1995).

Baddeleyite is relatively rare in nature, usually present in silica-undersaturated rocks, such as carbonatites, kimberlites, syenites, anorthosites, and some mafic and ultramafic rocks. It is also found in meteorites, lunar basalts and some Martian rocks (Heaman and LeCheminant 1993; Klemme and Meyer 2003; Rodionov et al. 2012). In contrast, zircon is widespread and occurs in a large variety of rocks, ranging from undersaturated to over-saturated igneous rocks, but it is most commonly found in igneous rocks of intermediate to silica-saturated compositions (Hoskin and Schaltegger 2003). Natural carbonatite may contain both baddeleyite and zircon as accessory minerals (e.g. Tichomirowa et al. 2013; Chakhmouradian et al. 2015). However, carbonatite zircons are usually large and well faceted and it has been suggested that many carbonatitic zircons may be xenocrysts (Barker 2001).

To investigate the respective stabilities of baddeleyite and zircon in carbonatites, we performed experiments in a range of different bulk compositions ranging from Ca-rich carbonate and silica-free melts to more complex Ca-rich silica-rich carbonate melts. Our aim was to constrain the stability fields of both baddeleyite and zircon in a simplified carbonatite system as a function of temperature and silica concentration in the melt.

Methods

Starting materials

The starting materials consist of haplo-carbonatite mixtures (Table 1). Eight different starting materials were prepared with analytical grade material: $CaCO_3$, Na_2CO_3, SiO_2, $4MgCO_3Mg(OH)_2$ and $Zr(OH)_2CO_3$, sourced from Merck and Alfa Aesar. The starting material compositions range from high-CaO and silica-free systems to high SiO_2 and low CaO compositions, with their $(CaO+MgO+Na_2O)/SiO_2$ ranging from 0.5 to 11.1. Trace elements were added to the starting material mixtures as standard solutions (Zr, Hf, Nb, Ta, Ti, Th, U, P, Rb, Sr, Ba, Cs, La, Ce, Sm, Nd, Yb, Lu, Pb, V, Sc, Mo, W) in concentrations of 100 µg/g

each. To prepare the starting materials, oxides and carbonates were mixed and ground in an agate mortar under acetone for 30 min.

Experiments

All experiments were performed in an end-loaded piston cylinder apparatus (Boyd and England 1960) at the Institut für Mineralogie, Münster University. The piston cylinder assembly consists of two inner cylinders made of crushable alumina (6 mm O.D.), and one cylinder made of boron nitride (6 mm O.D., 2 mm I.D), into which the capsule was inserted. The inner parts of the assembly are surrounded by a thin graphite furnace and outer Duran (Schott, Germany) glass and talc sleeves. Around 2 or 3 mg of starting material were sealed in Pt-capsules (2 mm O.D. and ca. 2.2 mm in length) using a PUK 3 Professional arc welder (Lampert Werktechnik GmbH, Germany). Most experiments were run with two capsules. Due to the large amount of low viscosity melt in most experiments, several preliminary runs leaked and were not used in this study. All experiments were performed at 0.7 GPa for 24 or 48 hours at temperatures of either 1000 °C or 1200 °C (Table 2). The chemical composition of the system forced us to run the experiments at these temperatures as runs at T<1000°C would be subsolidus.

The temperatures were measured by $W_{97}Re_3$–$W_{75}Re_{25}$ thermocouples and controlled with a Eurotherm controller. The samples were quenched by cutting off the electrical power, which caused the temperature to drop to 100°C in less than five seconds. A pressure correction of -10% calibrated on the quartz–coesite transition (Bose and Ganguly 1995) and the $MgCr_2O_4+SiO_2 = MgSiO_3+Cr_2O_3$ reaction (Klemme and O'Neill 1997) was applied. As most experiments were synthesis runs, we performed a few experimental reversal zircon dissolution runs (Harrison and Watson 1983; Gervasoni et al. 2016), in which cubes of a natural zircon crystal (0.8 mm side length, origin: Burma) were immersed in two melt compositions, CaMix15-D and CaMix16-D (Table 1). For these experiments, we used larger 2

mm O.D. and 4 mm long $Au_{80}Pd_{20}$ capsules. The reversal dissolution experiments were run for 72 h at 1200 °C and 0.7 GPa.

Analytical Methods

A Scanning Electron Microscope (SEM) JEOL 6610LV with an EDX system was used to characterize the run products. Major and minor element concentrations of the quenched carbonatite melt, silicate glasses and minerals were measured using JEOL JXA-8900 and JEOL JXA-8530F microprobes at the Insitut für Mineralogie, Münster University. The quenched melts were analyzed using an acceleration voltage of 15 kV, a beam current of 10 nA and a beam size of 10 to 20 μm diameters. Counting times for all elements were 5 s on the peak and 2.5 s on the background. Crystals were analyzed with a beam current of 15 nA and a beam varying from 5 to 10 μm according to the size of the crystal. The counting time of each element during the crystal analysis was 10 s (peak) and 5 s (background) except for Na which was analyzed for 5 and 2.5 s respectively. For better characterization of the mineral baghdadite ($Ca_3ZrSi_2O_9$) that was found in CaExp38 and CaExp39, Raman spectroscopic analysis was performed using a Jobin-Yvon LabRam HR800 spectrometer with a 532 nm wavelength laser at the Institute for Physical Chemistry, Münster University. The spectrum was obtained by averaging two spectra with an acquisition time of 30 s in frequency ranges between 120 to 1800 cm^{-1} and 3000 to 3800 cm^{-1} to search for O-H vibrations.

Experimental results

In general, run products consist of quenched Ca-rich carbonate melt, or a quenched Ca-rich silicate-carbonate melt (SiO_2 > 20 wt.%), each coexisting with various crystalline phases (Fig. 1; Table 2). The Ca-rich carbonate melts show typical dendritic quench textures consisting of swarms of elongated crystals (Fig. 1a, b, c, d), distinctly different to the silicate-carbonate melts which quench to a homogeneous glass (Fig. 1e, f).

The compositions of the Ca-rich carbonate melts are homogeneous throughout the capsule when measured with a 20 μm sized beam (Table S1). Melt compositions have CaO/SiO_2 ranging from 0.5 to 8.3 according to the bulk SiO_2 concentration of the system. Melt compositions range from low-silica carbonate melts with 40-50 wt.% CaO and 25-45 wt.% CO_2 to Ca-rich silicate-carbonate melts, with about 30 wt.% CaO, 30 wt.% SiO_2 and less than 25 wt.% CO_2. It is important to stress that the CO_2 concentrations of melts were calculated from the difference between measured EMP totals and 100 %. Baddeleyite occurs in almost all runs in contrast to zircon that was found only in SiO_2-rich melts. Some experiments contain wollastonite ($CaSiO_3$), baghdadite ($Ca_3ZrSi_2O_9$), $Ca_2ZrSi_4O_{12}$, clinopyroxene and natrite (Na_2CO_3) (Table 2). The average composition of the phases present in our run products are given in Table S2.

Experiments at 1000 °C

Four experiments were performed at 1000 °C. The melts in these experiments had CaO/SiO_2 ranging from 1.7 to 5.2 (Table S1). **Baddeleyite,** with sizes ranging from 1-10 μm, crystallized in melts that has low SiO_2 bulk composition (CaExp 32) (Tables 2 and S1). In two further experiments, baddeleyite occurs as inclusions in baghdadite (Fig. 1a). **Zircon** is present at 1000°C only in run CaExp41 (Table 2 and S1) and it is euhedral with sizes ranging from 1-15 μm (Fig. 1b). Some zircon crystals contain small inclusions of baddeleyite. **Wollastonite** occurs in all experiments at 1000°C as euhedral crystals, usually ranging from 20 up to 100 μm in size (Fig. 1a, b). Wollastonite sometimes contains small inclusions of baddeleyite, zircon or baghdadite. **Baghdadite** occurs in runs CaExp38 and CaExp39 at 1000°C and the crystals are euhedral, 20-100 μm in size and commonly contain inclusions of baddeleyite (Fig. 1a). **Clinopyroxene** occurs only in one experiment next to wollastonite crystals, with sizes of 5 to 10 μm (Fig. 1a). Minor quench natrite (**Na_2CO_3**) crystals occur in CaExp39, CaExp40 and CaExp41, interpreted to have formed as an immiscible phase from the Ca-rich silicate-carbonate melt. The natrite crystals are rectangular and 5-30 μm in size.

Experiments at 1200 °C

Baddeleyite occurs in almost all run products at 1200 °C (Table 2). The crystals are 1-10 μm in size and euhedral in low-SiO_2 carbonate melts (Fig. 1c, d) and anhedral with a rounded shape in melts with higher SiO_2 concentrations (Fig. 1e). Zircon is present in six experiments, in five of them coexisting with baddeleyite and wollastonite (Fig. 1e) (Table 2). Zircon occurs as subhedral to euhedral crystals. Their sizes range from 1-20 μm, and they often contain baddeleyite as an inclusion (Fig. 1e, f). **Wollastonite** occurs in five experiments at 1200°C together with baddeleyite and zircon (Table 2). Wollastonite is euhedral in our runs and 5-30 μm in size (Fig. 1e). We also find euhedral to subhedral **$Ca_2ZrSi_4O_{12}$** crystals in run CaExp 58, in sizes from 10-30 μm.

The zirconosilicates baghdadite and $Ca_2ZrSi_4O_{12}$

Baghdadite is a Ca-Zr silicate which was first found in a melilite skarn in the Qala-Dizeh region, Iraq (Al-Hermezi et al. 1986). It is a rare mineral that belongs to the cuspidine group (Dul et al. 2014), and it was also found in skarns from Japan, Norway, and Russia (Jamtveit et al. 1997; Matsubara and Miyawaki 1999; Shiraga et al. 2001; Galuskin et al. 2007) and in metamorphosed carbonatites from the Canary Islands (Casillas et al. 2008). Al-Hermezi et al. (1986) suggested that baghdadite was a product of the reaction of calcite and wollastonite with a Zr-rich melt, following the reaction: $2CaSiO_3 + CaCO_3 + ZrO_2$ (liq.) → $Ca_3ZrSi_2O_9 + CO_2$. However, we cannot comment on the origin of natural baghdadite but considering the rarity of this mineral, we characterized the crystals in our runs using Raman spectroscopy (Fig. 2a). When we compare the Raman spectrum of our experimental high-temperature baghdadite with the synthetic baghdadite studied by Dul et al. (2015) we find generally good agreement, except the peaks related to H-O bonds and C-O bonds found in our crystals.

The other rare zirconosilicate phase present in one of our experiments is $Ca_2ZrSi_4O_{12}$ (Kordyuk and Gulko 1962), which occurred at 1200°C and 0.7 GPa. $Ca_2ZrSi_4O_{12}$ is a

cyclosilicate (Vetsuki et al. 1985; Colin et al. 1993) which has not been reported in nature, yet. However, we suggest that $Ca_2ZrSi_4O_{12}$ should be stable in SiO_2-rich carbonatites with a significant Zr-content. The Raman spectrum of this phase is given in Figure 2b and may help to identify naturally occurring $Ca_2ZrSi_4O_{12}$. To our knowledge, no Raman spectrum of this phase has been published.

Reversal zircon dissolution experiments

To test the results of our synthesis experiments, additional dissolution experiments were performed in which small cubes of a natural gem quality zircon crystal were immersed in two different melt compositions, namely a SiO_2-free Ca-rich carbonate melt (run CaMix15-D) and a Ca-rich silicate-carbonate melt with 17 wt.% SiO_2 (CaExp16-D).

The results show that in a silica-free carbonatite composition (CaExp 59-D) the zircon cube was partially dissolved and replaced by baddeleyite and melt (Fig. 3a). The significant dissolution of zircon in a silica-free Ca-rich carbonate melt shows that zircon cannot be stable in such silica-poor melts. The final equilibrated melt in this run contains 32.8 wt.% SiO_2 and 6.3 wt.% ZrO_2 (Fig. 4b, Table S1), which is very similar to the melts of the synthesis experiments which contain both baddeleyite and zircon (CaExp 25, 29, 40, 55, 61). In run CaExp60-D, the zircon cube was immersed in a melt initially containing 17 wt.% SiO_2. The final equilibrated melt is found only very close to the partially dissolved cube (Fig. 3b) and its composition is much higher in SiO_2 (42.1 wt.%) (Fig. 4b, Table S1) and lower in ZrO_2 (0.9 wt.%) compared to CaExp59-D. Baddeleyite crystals grow on the rim of the zircon cube directly in contact with the melt. Zircon dissolution and subsequent recrystallization can also be observed in CaExp60-D (Fig. 3b). Melts from both dissolution experiments are further characterized by low CaO contents (2-3 wt.%) compared to the CaO content of the starting material (30-40% CaO). In summary, the results from our reversal zircon dissolution experiments agree well with the synthesis experiments (Table S1).

The stability of baddeleyite and zircon in silica-bearing carbonate melts

Figure 4 depicts the melt compositions of our run products at different temperatures in terms of SiO_2 and ZrO_2. At 1000°C (Fig. 4a), baddeleyite crystallizes in Ca-rich carbonate melts with less than 10 wt.% SiO_2 and a high CaO/SiO_2 ratio of 5.2. In contrast, zircon occurs in our experiments together with wollastonite only in melts with higher SiO_2 concentrations, i.e. SiO_2>20 wt.% and CaO/SiO_2= 1.7. Baghdadite and wollastonite crystallize together in melts with 13.9 and 15.8 wt.% of SiO_2 and CaO/SiO_2 of 2.8 and 2.3, respectively. Baghdadite is a zirconosilicate phase that occurs in our experiments only in intermediate melts (in terms of silica) between the stability field of baddeleyite and zircon (Fig. 4a). The presence of baghdadite instead of zircon in low-silica carbonate melts (i.e., SiO_2 <20 wt.%), shows that zircon indeed needs high silica concentrations in melts to crystallize.

At 1200 °C, baddeleyite occurs in almost all runs in equilibrium with melts with SiO_2 ranging from 0-34.3 wt.%. At this temperature, baddeleyite is the only zirconium phase in melt compositions with SiO_2 lower than 20 wt.% (Fig. 4b). Zircon, on the other hand, occurs together with wollastonite and baddeleyite in Ca-rich silicate-carbonate melts with at least 30 wt.% of SiO_2 (Fig. 4b). To crystallize zircon without baddeleyite at 1200°C, the SiO_2 concentration of the melts must be higher than 40 wt.% and CaO/SiO_2 <1 (CaExp57 and CaExp58).

Discussion

The main aim of this study was to define the stability field of baddeleyite and zircon in carbonate melts with different SiO_2 concentrations, and hence, to understand the occurrence of baddeleyite, zircon, and other silicate minerals in silica-undersaturated rocks such as carbonatites. To address this question, we investigated experimentally the relative stability of baddeleyite (ZrO_2) and zircon ($ZrSiO_4$) in carbonate melts with different SiO_2-contents. However, crystallizing zircon in our experiments proved to be a challenge. Only eight of our run products contain zircon, and most of them also contain baddeleyite and wollastonite.

As most naturally occurring carbonatite melts are undersaturated in silica, baddeleyite should be the most abundant Zr-rich accessory mineral in these rocks, and it is indeed a prominent mineral in carbonatite. For instance, the Phalaborwa carbonatite contains large crystals of baddeleyite (e.g., Eriksson 1984; Heaman and LeCheminant 1993), but it is also common in other carbonatites such as at the Kovdor Massif in the Kola alkaline province in northern Russia (e.g., Rodionov et al. 2012) or the Mud Tank Complex in Australia (Hoskin and Schaltegger 2003). Nevertheless, zircon also occurs in the aforementioned carbonatites, and indeed in many others carbonatites, often as large and euhedral crystals.

Barker (2001) suggested that zircons either form as a primary phases in carbonatite magmas with high silica activity, or that zircons are entrained from other silicate magmas (parental or coeval), or as xenocrysts. Furthermore, he also suggested that zircon in carbonatite may be products of subsolidus alteration or accidental phases incorporated during subsolidus flow (Barker 1989, 1993). Our results may shed some further light on the origin of zircon in carbonatite, as they show that baddeleyite is stable in low-silica carbonate melts but zircon is stable only in more evolved Ca-rich silicate-carbonate melts with significant concentrations of SiO_2.

If a primary carbonate melts evolves towards higher SiO_2 contents by fractionation or contamination, our experiments suggest that baddeleyite crystallizes first, followed by baghdadite that crystallizes in melts of 13-14 wt.% SiO_2. Zircon crystallizes only in melts with at least 20 wt.% SiO_2 (Fig. 4 a, b). Moreover, if zircons in carbonatite are xenocrysts (Barker 2001), our experiments indicate that they cannot survive in a silica-poor melt for a long time without being dissolved (Fig. 3b; Run CaExp-60D).

The zircon saturation in these carbonate-rich systems is sensitive to temperature, resulting in a higher Zr concentration in melts with higher temperatures (Fig. 4 a, b). This is in good general agreement with other zircon saturation studies (Watson and Harrison 1983; Boehnke et al. 2013; Gervasoni et al. 2016). Marr et al. (1998) also studied the stability of Zr-

bearing phases in peralkaline melt compositions. According to their experiments, zircon crystallizes only in melts with at least 57-60 wt.% SiO_2, and peralkaline melts with lower SiO_2 crystallize wadeite ($K_2ZrSi_3O_9$) as the predominant Zr-bearing phase. Our results in carbonate-rich melts agree with this observation, as we find that the zirconosilicate baghdadite is stable in our experiments at 1000°C and this restricts zircon crystallization to melts with >20 wt.% SiO_2.Our experiments were done in a rather simple chemical composition, and addition of more components to the system would most likely stabilize an entirely different suite of accessory minerals, e.g. addition of Ti should stabilize calzirtite ($CaZr_3TiO_9$), zirconolite ($CaZrTi_2O_7$) or Zr-bearing perovskite ($CaTiO_3$).

In addition, several studies showed that zircons from carbonatite exhibit extreme variability in terms of trace element composition (Savva et al. 2010; Rodionov et al. 2012). This chemical variability may indicate that the zircon records the complex evolution of the evolving melts (Belousova et al. 1998, 2002; Chakhmouradian and Williams 2004; Rodionov et al. 2012). Therefore, care should be taken when using zircons for geochronology and other geochemical studies of carbonatites, as zircon in many carbonatites may not be a primary phase but most likely a phase that crystallized from a differentiated and evolved silica-rich magma.

Implications

We investigated the stability of baddeleyite and zircon in a variety of carbonate-rich melts, ranging from low-silica Ca-rich carbonate melt to Ca-rich silicate-carbonate melts. Our experiments show that the primary Zr-phase in low-silica carbonatites is baddeleyite. Baddeleyite crystallizes in Ca-rich carbonate melts with SiO_2 contents lower than 20 wt.% and in Ca-rich silicate-carbonate melts of at least 30 wt.% of SiO_2. Zircon does not occur in low-silica carbonate melts and only crystallizes when the melt evolves to Ca-rich silicate-carbonate compositions with at least 20 wt.% of SiO_2 at 1000 °C or 30 wt.% of SiO_2 at 1200

°C. Dissolution experiments also show that zircon cannot be a stable phase in silica-free carbonate melts, but it can only be stable in evolved melts with higher SiO_2 concentrations. Thus, we suggest that zircon in carbonatites crystallized from melts with high SiO_2 concentrations and that zircon found in SiO_2-poor carbonatites did not crystallize from a primary calciocarbonatite magma. Therefore, the use of zircon for geochronology and geochemical studies of carbonatites requires extra caution since zircon might not be a primary phase in such rocks. We would like to recommend using baddeleyite for dating of low-silica carbonatites as this is most likely the primary mineral in these rocks.

Acknowledgments

We would like to thank Maik Trogisch for his help with sample preparation and Beate Schmitte for her help with the electron microprobe analyses. Further thanks go to Dr. C. Sanchez-Valle for her help with the Raman Spectroscopy. Thanks also go to Dr. A.R. Chakhmouradian, an anonymous reviewer, and the editor for their helpful and constructive comments and suggestions. F. Gervasoni thanks the Brazilian CAPES foundation for a PhD scholarship (BEX 12363/12-0) in Germany.

References

Al-Hermezi, H.M., McKie, D., and Hall, A.J. (1986) Baghdadite, a new calcium zirconium silicate mineral from Iraq. Mineralogical Magazine, 50, 119–123.

Barker, D.S. (1989) Field relations of carbonatites. In K. Bell, Ed., Carbonatites: genesis and evolution pp. 38–69. Unwin Hyman, London.

Barker, D.S. (1993) Diagnostic magmatic features in carbonatites: implications for the origins of dolomite- and ankerite-rich carbonatites. South African Journal of Geology, 96, 131–138.

Barker, D.S. (2001) Calculated silica activities in carbonatite liquids. Contributions to

310 Mineralogy and Petrology, 141, 704–709.
311 Belousova, E.A., Griffin, W.L., and Pearson, N.J. (1998) Trace element composition and
312 cathodoluminescence properties of southern African kimberlitic zircons. Mineralogical
313 Magazine, 62, 355–366.
314 Belousova, E., Griffin, W., O'Reilly, S.Y., and Fisher, N. (2002) Igneous zircon: trace
315 element composition as an indicator of source rock type. Contributions to Mineralogy
316 and Petrology, 143, 602–622.
317 Boehnke, P., Watson, E.B., Trail, D., Harrison, T.M., and Schmitt, A.K. (2013) Zircon
318 saturation re-revisited. Chemical Geology, 351, 324–334.
319 Bose, K., and Ganguly, J. (1995) Quartz–coesite transition revisited - reversed experimental-
320 determination at 500–1200°C and retrieved thermochemical properties. American
321 Mineralogist, 80, 231–238.
322 Brooker, R.A., and Kjarsgaard, B.A. (2011) Silicate-carbonate liquid immiscibility and phase
323 relations in the system SiO_2-Na_2O-Al_2O_3-CaO-CO_2 at 0.1-2.5 GPa with applications to
324 carbonatite genesis. Journal of Petrology, 52, 1281–1305.
325 Casillas, R., Nagy, G., Demény, A., Ahijado, A., and Fernández, C. (2008) Cuspidine-
326 niocalite-baghdadite solid solutions in the metacarbonatites of the Basal Complex of
327 Fuerteventura (Canary Islands). Lithos, 105, 25–41.
328 Chakhmouradian, A.R., and Williams, T.C. (2004) Mineralogy of highfield-strength elements
329 (Ti, Nb, Zr, Ta, Hf) in phoscoritic and carbonatitic rocks of the Kola Peninsula, Russia.
330 In F. Wall and A.N. Zaitsev, Eds., Phoscorites and Carbonatites from Mantle to Mine:
331 the Key Example of the Kola Alkaline Province pp. 293–340. Mineralogical Society,
332 London.
333 Chakhmouradian, A.R., Reguir, E.P., Kressall, R.D., Crozier, J., Pisiak, L.K., Sidhu, R., and
334 Yang, P. (2015) Carbonatite-hosted niobium deposit at Aley, northern British Columbia
335 (Canada): Mineralogy, geochemistry and petrogenesis. Ore Geology Reviews, 64, 642–

666.

Colin, S., Dupre, B., Venturini, G., Malaman, B., and Gleitzer, C. (1993) Crystal Structure and Infrared Spectrum of the Cyclosilicate $Ca_2ZrSi_4O_{12}$. Journal of Solid State Chemistry, 102, 242–249.

Dobson, D., Jones, A., Rabe, R., Sekine, T., Kurita, K., Taniguchi, T., Kondo, T., Kato, T., Shimomura, O., and Urakawa, S. (1996) In-situ measurement of viscosity and density of carbonate melts at high pressure. Earth and Planetary Science Letters, 143, 207–215.

Dul, K., Kolezinski, A., Sitarz, M., and Madej, D. (2014) Vibrational spectra of a baghdadite synthetic analogue. Vibrational Spectroscopy, 76, 1–5.

Eriksson, S.C. (1984) Age of carbonatite and phoscorite magmatism of the Phalaborwa Complex (South Africa). Isotope Geoscience, 2, 291–299.

Galuskin, E.V., Pertsev, N.N., Armbruster, T., Kadiyski, M., Zadov, A.E., Galuskina, I.O., Dzierzanowski, P., Wrzalik, R., and Kislov, E. (2007) Dovyrenite $Ca_6Zr[Si_2O_7]_2(OH)_4$ - a new mineral from skarned carbonate xenoliths in basic-ultrabasic rocks of the Ioko-dovyren Massif, Northern Baikal Region, Russia. Mineralogia Polonica, 38, 15–28.

Gervasoni, F., Klemme, S., Rocha-Júnior, E.R.V., and Berndt, J. (2016) Zircon saturation in silicate melts: a new and improved model for aluminous and alkaline melts. Contributions to Mineralogy and Petrology, 171, 21.

Gittins, J. (1988) The origin of carbonatites. Nature, 335, 295–296.

Gittins, J., and Jago, B.C. (1998) Differentiation of natrocarbonatite magma at Oldoinyo Lengai volcano, Tanzania. Mineralogical Magazine, 62, 759–768.

Harmer, R.E., and Gittins, J. (1998) The case for primary, mantle-derived carbonatite magma. Journal of Petrology, 39, 1895–1903.

Harrison, T.M., and Watson, E.B. (1983) Kinetics of zircon dissolution and zirconium diffusion in granitic melts of variable water content. Contributions to Mineralogy and Petrology, 84, 66–72.

362 Heaman, L.M., and LeCheminant, A.N. (1993) Paragenesis and U-Pb systematics of
363 baddeleyite (ZrO_2). Chemical Geology, 110, 95–126.
364 Hoskin, P.W.O., and Schaltegger, U. (2003) The composition of zircon and igneous and
365 metamorphic petrogenesis. Reviews in Mineralogy and Geochemistry, 53, 27–62.
366 Jamtveit, B., Dahlgren, S., and Austrheim, H. (1997) High-grade contact metamorphism of
367 calcareous rocks from the Oslo Rift, Southern Norway. American Mineralogist, 82,
368 1241–1254.
369 Kjarsgaard, B., and Hamilton, D. (1988) Liquid immiscibility and the origin of alkali-poor
370 carbonatites. Mineralogical Magazine, 43–55.
371 Klemme, S., and Meyer, H.P. (2003) Trace element partitioning between baddeleyite and
372 carbonatite melt at high pressures and high temperatures. Chemical Geology, 199, 233–
373 242.
374 Klemme, S., and O'Neill, H.S.C. (1997) The reaction $MgCr_2O_4 + SiO_2 = Cr_2O_3 + MgSiO_3$
375 and the free energy of formation of magnesiochromite ($MgCr_2O_4$). Contributions to
376 Mineralogy and Petrology, 130, 59–65.
377 Klemme, S., van der Laan, S.R., Foley, S.F., and Günther, D. (1995) Experimentally
378 determined trace and minor element partitioning between clinopyroxene and carbonatite
379 melt under upper mantle conditions. Earth and Planetary Science Letters, 133, 439–448.
380 Kono, Y., Kenney-Benson, C., Hummer, D., Ohfuji, H., Park, C., Shen, G., Wang, Y.,
381 Kavner, A., and Manning, C.E. (2014) Ultralow viscosity of carbonate melts at high
382 pressures. Nature communications, 5, 5091.
383 Le Maitre, R.W., Ed. (2002) Igneous Rocks: a classification and glossary of terms. Cambridge
384 University Press, Cambridge, U.K.
385 Mariano, A.N. (1989) Nature of economic mineralization in carbonatites and related rocks. In
386 K. Bell, Ed., Carbonatites: genesis and evolution pp. 428–447. Unwin Hyman, London.
387 Matsubara, S., and Miyawaki, R. (1999) Baghdadite from the Akagane mine, Iwate

Prefecture, Japanese Bulletin of the National Science Museum, Serie C, 25, 65–72.

Minarik, W.G., and Watson, E.B. (1995) Interconnectivity of carbonate melt at low melt fraction. Earth and Planetary Science Letters, 133, 423–437.

Mitchell, R.H. (2005) Carbonatites and carbonatites and carbonatites. The Canadian Mineralogist, 43, 2049–2068.

Marr, R.A., Baker, D.R., Williams-Jones, A.E. (1998) Chemical controls on the solubility of Zr-bearing phases in simplified peralkaline melts and application to the Strange Lake Intrusion, Quebec-Labrador. The Canadian Mineralogist, 36, 1001-1008.

Reischmann, T., Brügmann, G.E., Jochum, K.P., and Todt, W.A. (1995) Trace element and isotopic composition of baddeleyite. Mineralogy and Petrology, 53, 155–164.

Rodionov, N. V., Belyatsky, B. V., Antonov, A. V., Kapitonov, I.N., and Sergeev, S.A. (2012) Comparative in-situ U-Th-Pb geochronology and trace element composition of baddeleyite and low-U zircon from carbonatites of the Palaeozoic Kovdor alkaline-ultramafic complex, Kola Peninsula, Russia. Gondwana Research, 21, 728–744.

Savva, E.V., Belyatsky, B.V., and Antonov, A.V. (2010) Carbonatitic zircon — geochemical analysis Vol. 6, p. 576. Acta Mineralogica-Petrographica, Abstract Series.

Shiraga, K., Kusachi, I., Kobayashi, S., and Yamakawa, L. (2001) Baghdadite from Fuka, Okayama Prefecture, Japan. Journal of Mineralogical and Petrological Sciences, 96, 43–47.

Sweeney, R.J. (1994) Carbonatite melt compositions in the Earth's mantle. Earth and Planetary Science Letters, 128, 259–270.

Tichomirowa, M., Whitehouse, M.J., Gerdes, A., Götze, J., Schulz, B., and Belyatsky, B.V. (2013) Different zircon recrystallization types in carbonatites caused by magma mixing: Evidence from U–Pb dating, trace element and isotope composition (Hf and O) of zircons from two Precambrian carbonatites from Fennoscandia. Chemical Geology, 353, 173–198.

Wallace, M.E., and Green, D.H. (1988) An experimental determination of primary carbonatite magma composition. Nature, 335, 343–346.

Watson, E.B., and Harrison, T.M. (1983) Zircon saturation reviseted: temperature and composition effects in a variety of crustal magmas types. Earth and Planetary Science Letters, 64, 295–304.

Yaxley, G.M., Crawford, A.J., and Green, D.H. (1991) Evidence for carbonatite metasomatism in spinel peridotite xenoliths from western Victoria, Australia. Earth and Planetary Science Letters, 107, 305–317.

List of Figures

Figure 1. Back-scattered electron images of representative experimental run products. a) Run CaExp38: wollastonite, baghdadite and clinopyroxene in a quenched carbonatite with 15.8 wt.% SiO_2 at 1000 °C; wollastonite and baghdadite form euhedral crystals; baghdadite often contains baddeleyite as inclusions; clinopyroxene is euhedral and occurs in contact with wollastonite; b) Run CaExp41: euhedral zircon and wollastonite crystallized in a quenched Ca-rich silicate-carbonate melt with 20 wt.% SiO_2 at 1000 °C; some zircon crystals contain submicron-sized inclusions of baddeleyite; c) Run CaExp7: euhedral baddeleyite crystallized in a quenched carbonatite melt with no SiO_2 at 1200 °C; d) Run CaExp12: euhedral baddeleyite crystallized in a quenched carbonatite melt with 5.2 wt.% SiO_2 at 1200 °C; e) Run CaExp40: zircon, baddeleyite and wollastonite crystallized in a Ca-rich silicate-carbonate melt with 31.7 wt.% SiO_2 at 1200 °C; zircons are euhedral and contain baddeleyite and wollastonite inclusions, baddeleyite exhibits a rounded shape typical for our run products with Ca-rich silicate-carbonate melt. Wollastonite is usually euhedral, and a few pools exist with Na-fluids; f) Run CaExp 57: small and euhedral zircons crystallized in a Ca-rich silicate-carbonate melt with 40.6 wt.% SiO_2 at 1200 °C; some zircon crystals contain small baddeleyite inclusions; fluid pools are Na-rich in composition.

Figure 2. Raman spectrum of the mineral baghdadite (a) in run CaExp 38 and the crystalline phase $Ca_2ZrSi_4O_{12}$ (b) in run CaExp58.

Figure 3. Back-scattered electron images of the zircon dissolution experiments. a) Run CaExp59-D: A silica-free carbonatite melt causes zircon replacement by baddeleyite and melt; b) Run CaExp60-D: zircon has only been partially dissolved by a silicate-carbonate melt (CaMix16-D). Baddeleyite crystallized at the zircon rims which was in contact with the melt.

Figure 4: Accessory phase stability in different experimental melt compositions: a) at 1000 °C; b) at 1200 °C. At 1000°C baddeleyite is stable in melts with 0-13 wt.% SiO_2 and zircon is stable in melts with more than 17% SiO_2. At 1000 °C, there is an intermediate stability field of wollastonite and baghdadite. At 1200°C, baddeleyite is stable in melts with 0-25 wt.% SiO_2 and zircon is stable in melts with more than 40 % SiO_2. In melts with around 30% SiO_2 baddeleyite, zircon and wollastonite crystallize in our experiments. Abbreviations: badd=baddeleyite; zrn=zircon; woll=wollastonite; baghda=baghdadite. The dashed lines are handdrawn to separate stability fields of baddeleyite and zircon.

Tables

Table 1. Starting material compositions (wt.%)

	CaMix6	**CaMix7**	**CaMix8**	**CaMix9**	**CaMix10**	**CaMix11**	**CaMix13**	**CaMix14**	**CaMix15-D***	**CaMix16-D***	**Wollastonite**
CaO	39	37	36	33	29	31	25	18	45	37	48
Na_2O	8	7	7	6	6	6	5	2	9	7	-
MgO	2	2	2	2	1	1	1	1	2	2	-
SiO_2	0	4	8	15	26	21	28	45	0	17	52
ZrO_2	10	10	10	9	8	8	13	14	0	0	-
CO_2	40	38	36	34	29	31	26	19	43	36	-
H_2O	2	2	1	1	1	1	2	2	1	1	-
Total	100	100	100	100	100	100	100	100	100	100	100
$(CaO+MgO+Na_2O)/SiO_2$	-	11.1	5.6	2.8	1.4	1.9	1.1	0.5	-	2.8	-

*CaMix15-D and CaMix16-D are starting materials used in ‘reversal’ zircon dissolution experiments.

460 Table 2. Experimental run conditions and results

Runs	Starting material	P (Gpa)	T°C	Time (h)	Badd and/or Zrn	Other phases
CaExp07	CaMix6	0.7	1200	24	Badd	Lc
CaExp11	CaMix6	0.7	1200	24	Badd	Lc
CaExp12	CaMix7	0.7	1200	24	Badd	Lc
CaExp13	CaMix8	0.7	1200	24	Badd	Lc
CaExp14	CaMix8	0.7	1200	24	Badd	Lc
CaExp24	CaMix9	0.7	1200	24	Badd	Ls
CaExp25	CaMix10	0.7	1200	24	Zrn+badd	Woll+Ls
CaExp26	CaMix7	0.7	1200	24	Badd	Lc
CaExp28	CaMix9	0.7	1200	24	Badd	Ls
CaExp29	CaMix10	0.7	1200	24	Zrn+badd	Woll+Ls
CaExp40	CaMix11	0.7	1200	24	Zrn+badd	Woll+Ls
CaExp42	CaMix9	0.7	1200	24	Badd	Ls
CaExp55	CaMix13	0.7	1200	24	Zrn+badd	Woll+Ls
CaExp57	CaMix14+Woll	0.7	1200	24	Zrn	Ls
CaExp58	CaMix14	0.7	1200	24	Zrn	Woll+$Ca_2ZrSi_4O_{12}$+Ls
CaExp61	CaMix13+Woll	0.7	1200	24	Zrn+Badd	Woll+Ls
CaExp32	CaMix9	0.7	1000	24	Badd	Woll+Lc
CaExp38	CaMix8	0.7	1000	48	-	Woll+Baghda+Cpx+Na_2CO_3+Lc
CaExp39	CaMix9	0.7	1000	48	-	Woll+Baghda+Na_2CO_3+Lc
CaExp41	CaMix11	0.7	1000	48	Zrn	Woll+Na_2CO_3+Lc
CaExp59-D	CaMix15-D*	0.7	1200	72	Zrn+Badd	Ls
CaExp60-D	CaMix16-D*	0.7	1200	72	Zrn	Ls

461

462 Badd = baddeleyite; Zrn = zircon; Woll = wollastonite; Baghda = baghdadite ($Ca_3ZrSi_2O_9$);
463 Cpx = clinopyroxene; $Ca_2ZrSi_4O_{12}$; Na_2CO_3; Lc = quenched carbonate melt; Ls = quenched
464 silicate-carbonate melt. The CaExp57 was run with a mixture of 90% CaMix14 + 10%
465 wollastonite component and CaExp61 was run using a mixture of 90% CaMix13 + 10%
466 wollastonite component. Dissolution experiments (CaExp59-D and CaExp60-D) were
467 performed with their respective starting materials (Table 1) and a zircon cube of 0.8 mm side
468 length.

469

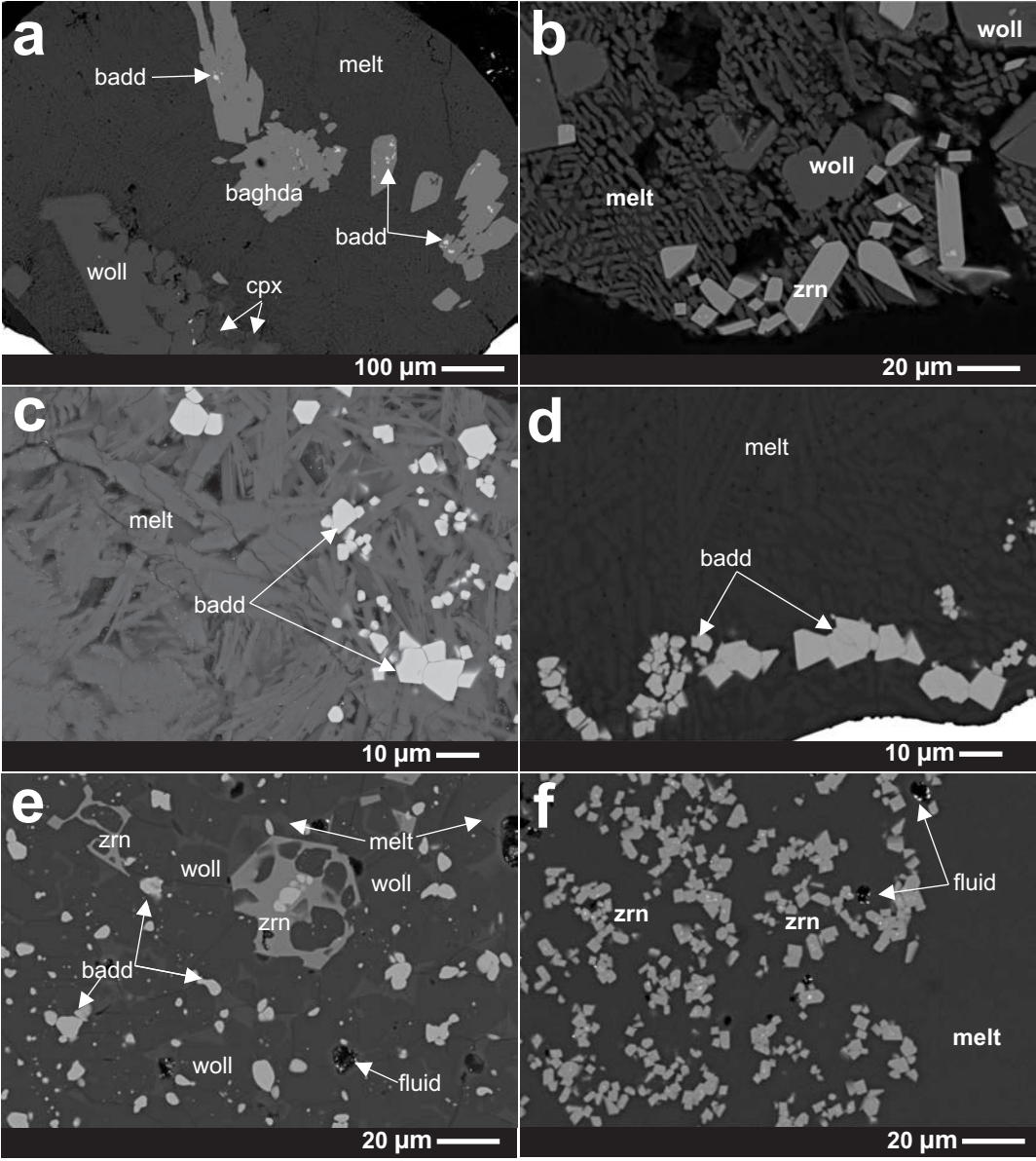
a
badd
melt
baghda
badd
woll
cpx
100 µm
b
woll
woll
melt
zrn
20 µm
c
melt
badd
10 µm
d
melt
badd
10 µm
e
zrn
melt
woll
woll
zrn
badd
woll
fluid
20 µm
f
fluid
zrn
zrn
melt
20 µm

Fig 1

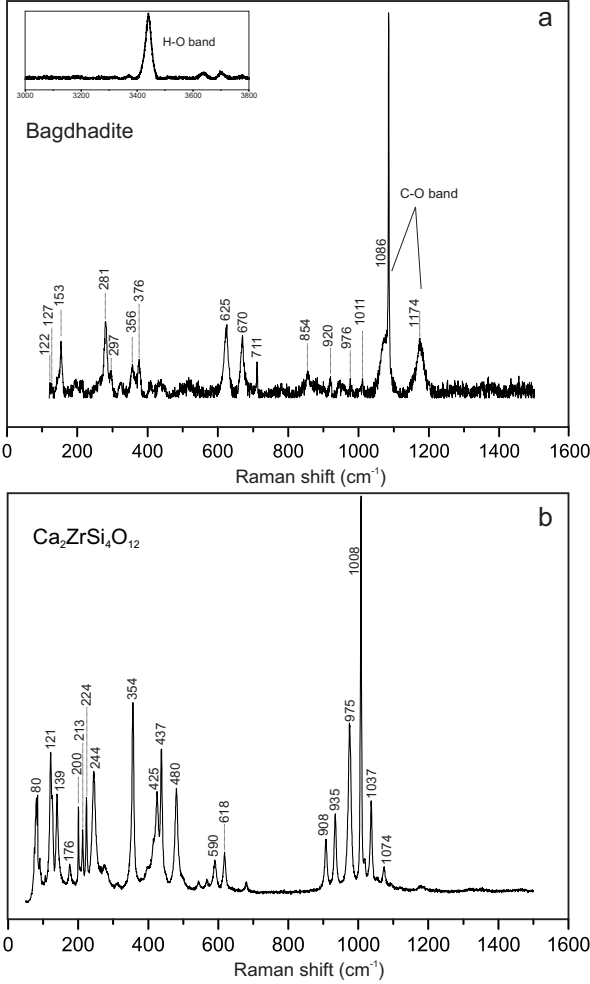
a
H-O band
3000
3200
3400
3600
3800
Bagdhadite
C-O band
1086
122
127
153
281
297
356
376
625
670
711
854
920
976
1011
1174
0
200
400
600
800
1000
1200
1400
1600
Raman shift (cm-1)
b
Ca2ZrSi4O12
1008
80
121
139
176
200
213
224
244
354
425
437
480
590
618
908
935
975
1037
1074
0
200
400
600
800
1000
1200
1400
1600
Raman shift (cm-1)

Fig 2

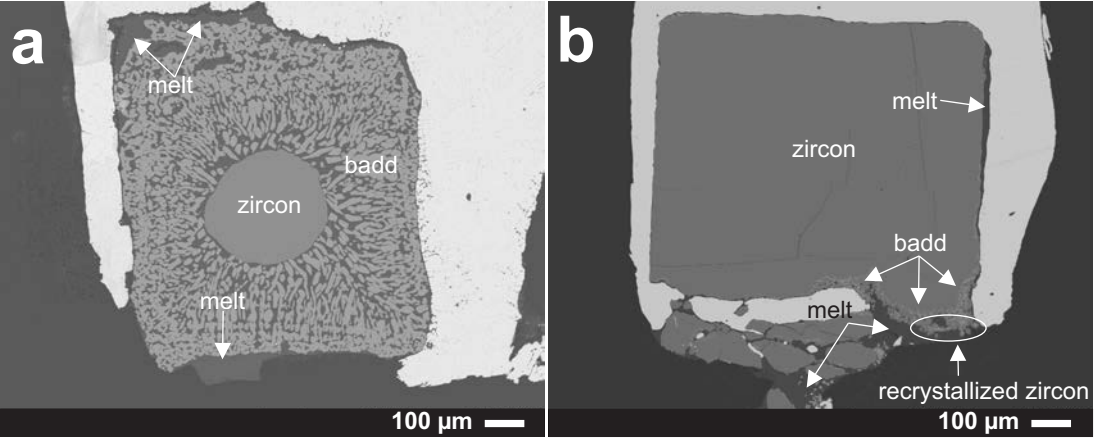
a
melt
badd
zircon
melt
100 µm
b
melt
zircon
badd
melt
recrystallized zircon
100 µm

Fig 3

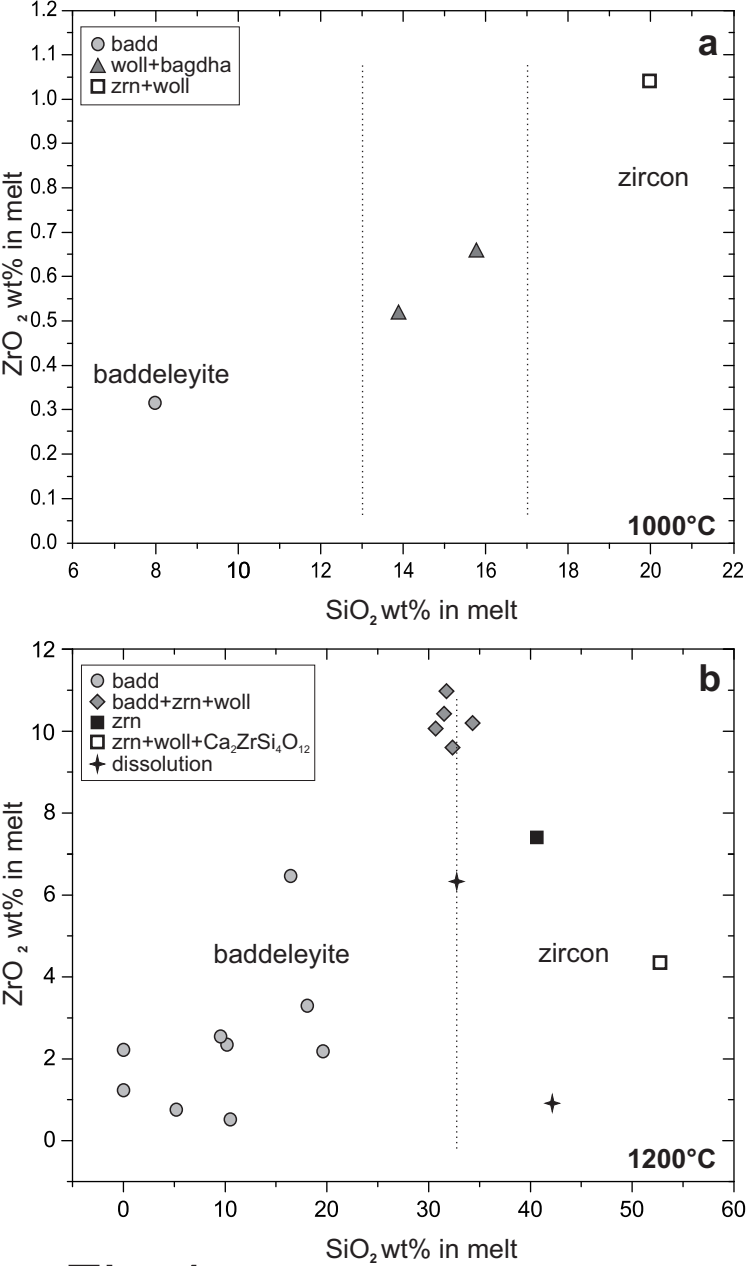
badd
woll+bagdha
zrn+woll
a
zircon
baddeleyite
1000°C
ZrO 2 wt% in melt
SiO2 wt% in melt
badd
badd+zrn+woll
zrn
zrn+woll+Ca2ZrSi4O12
dissolution
b
baddeleyite
zircon
1200°C
ZrO 2 wt% in melt
SiO2 wt% in melt

Fig 4